Resonant Turbulence applied to a Low Swirl Burner

A.A. Verbeek[1,*], R.C. Pos[1], G.G.M. Stoffels[1], Th.H. van der Meer[1]

[1] Laboratory of Thermal Engineering, University of Twente, P.O. Box 217, 7500 AE, Enschede, The Netherlands

Abstract Is it possible to optimize the turbulent combustion of a low swirl burner by using resonance in turbulence? To answer that question an active grid with periodically opening and closing holes is constructed and placed upstream of a burner geometry. The presence of this grid introduces large scale turbulent fluctuations to the flow with frequencies related to the driving frequency of the active grid. It is investigated what the optimum frequency is to excite the flow to obtain enhanced turbulence. First results show a response maximum of the eddy dissipation rate when the frequency of the introduced turbulent fluctuations is close to the inverse of the large eddy turn over time, which is also predicted by several numerical and experimental studies.

Introduction

A clean and efficient way of generating heat and momentum by combustion is to operate in the lean premixed regime. While lean combustion results in low NOx emissions, low CO and low un-burnt hydrocarbons, it also reduces the stability of the combustion. Here the need for proper flame stabilization emerges. The conventional method is the high swirl stabilization concept. Here the strong swirling flow generates a post-flame recirculation zone, where fresh reactants are continuously ignited by a back-flow of hot combustion products. Although this stabilization mechanism has been very successful and is used in many gas turbine applications [1] the remaining NOx formation cannot be reduced further due to the relative high residence time caused by the recirculation.

A newly invented stabilization mechanism avoids the necessity for a recirculation zone [2]. This so called low swirl burner has a lower swirl which is not strong enough to form the recirculation zone. Due to the tangential velocity a diverging flow pattern is created at the burner outlet as can be seen in the left picture of figure 1. The right picture of figure 1 shows the geometry of a low swirl burner. It consists of an outer annulus with tilted vanes to cause the outer flow to gain tangential velocity and an inner section with a blocking grid to balance the central and outer swirling flow and to generate some turbulence. Downstream of the swirler there is a short settling section of 1 to 1.5 times the diameter before the gases exit the burner tube.

The flame stabilizes in the diverging flow at the location where the turbulent flame speed equals the local fluid velocity. In absence of the recirculation zone the formation of NOx will primarily depend on the flame temperature [3]. Although the low swirl stabilization concept is able to reduce NOx emissions with 60% [3], there is limited turbulent mixing, as can be seen in figure 1 from the little shear stress in the central region. To increase the flame surface density and make the flame more compact and robust the turbulent mixing should be increased.
In this project it is investigated how the turbulent mixing

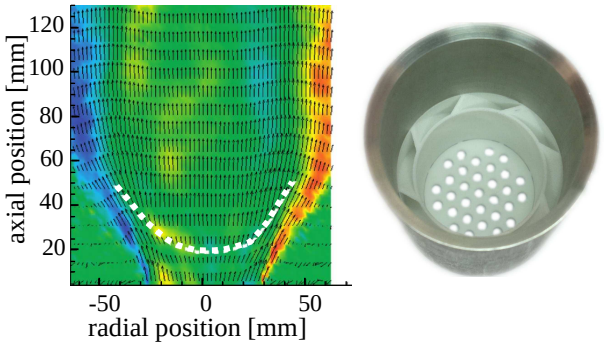

Figure 1: Left: Flow field of low swirl burner. The white dashed line indicates the location of flame. The color indicates the magnitude of the shear stress[4]. Right: Photograph of low swirl burner geometry.

can be increased by a modulated agitation of the flow upstream. This modulated agitation is suggested by several numerical studies [5, 6] where the excitation is modulated in time and applied only to the larger scales. Here a large scale forcing is applied; not with a constant value but with a periodic modulation added to it. The flow will respond different to different frequencies of the periodic modulation. At low frequency the flow can follow the modulation, but at high frequencies the response amplitude tends to decrease with the reciprocal of the frequency. In between, at roughly the inverse of the large eddy turnover time a response maximum is found.
Experimental observations also confirm this resonant enhancement of the turbulence. Cadot et al. [7] found in their counter rotating disk experiment a response maximum of the turbulent kinetic energy and Cekli et al. [8] observed a response maximum in the eddy dissipation rate when the active grid is forcing the flow at a specific frequency. In both cases the response maximum is located in the order of the inverse of the large eddy turn over time. In order to achieve this large scale time modulated forcing in a burner geometry the concept of an active grid [9] as used in wind tunnel experiments is used. The location and time dependent permeability in an active grid by means of several individual controlled axes,

*Corresponding author: a.a.verbeek@utwente.nl

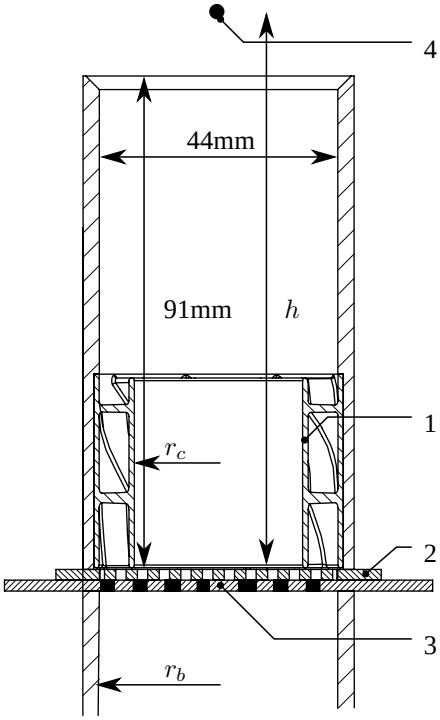

Figure 2: Cross section of the active grid upstream of the swirler geometry with global dimensions. 1: Insertable swirler geometry. 2: Static perforated disk. 3: Rotating disk. 4: Location of the hot-wire probe.

can also be obtained by using a rotating plate with the right perforations. This is explained in the next section. The work presented in this paper reports on the progress of obtaining resonant turbulence in a burner geometry.

Experimental setup

The burner that is studied in this project is a 50kW thermal power low swirl burner based on the design guidelines described by Cheng and Levinsky [4]. As can be seen in figure 2 there is an insertable swirler that can be replaced to study the effect of parameters like swirl number and the mass flow ratio between the central section and the outer annulus.

The design used in the experiments reported here has the following characteristics:

- Swirl $S = 0.45$
- Vane angle $\alpha = 37.5$
- Center to burner radius $r = r_c/r_b = 0.77$

In order to have a reasonable turn down ratio (5:1) the outer radius of the burner is set to 22mm. At maximum power and at an equivalence ratio of 0.7 the 6Nm^{3}n natural gas is combusted with 72Nm^3 air resulting in a velocity of 14m/s. The power can be decreased until the fluid velocity is approximately 3m/s for safety reasons.

Before the active grid there is straight tube of one meter length with a flow conditioner at the inlet to suppress

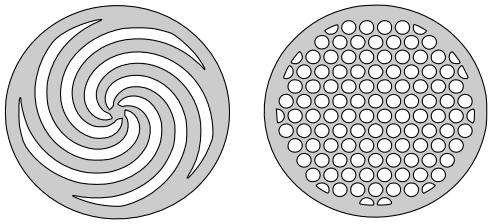

Figure 3: Drawing of the used disks to create an active grid. Left: Rotating disk with five spiral shaped slots. The width of the slots is 3mm. Right: Static disk with 3mm perforations in a hexagonal pattern. The distance between two adjacent holes is 1 mm.

flow irregularities like swirl and an asymmetrical velocity distribution. The flow conditioner is constructed by means of an orifice plate with an opening diameter of 14mm.

The natural gas and the combustion air are brought together upstream of the straight settling section in a venturi mixer where it subsequently passes through a helical static mixer to ensure proper mixing. The air flow is controlled by setting the upstream pressure of a calibrated sonic nozzle and the natural gas flow is controlled with an electronically controlled proportional valve.
In order to obtain a periodic forcing of the flow an active grid is constructed with perforations that are periodically opening and closing. In this way every hole forms a pulsating jet. One way to obtain this phenomenon is the use of a rotating disk with spiral shaped slots in front of a static perforated plate. In figure 3 the two used disks are depicted. The spiral shaped slot will open every perforation one time per revolution, so the five slots will create a pulsating jet at every perforation with a frequency of five times the rotation frequency.

In order to let the disk rotate, the tube is divided into two parts as can be seen in figure 2. The rotating disk extends out of it and is mounted on a rotating ring that is driven with a V-belt and an AC-motor. While the actual rotation speed is measured by an optical encoder, the motor rotation speed is set by an analog voltage signal sent from the control PC to an AC frequency controller. A PID control loop makes sure that the disk is rotating at the desired set point with a precision better than 0.1Hz. The maximal rotation speed is 35Hz.

Besides the creation of pulsating jets, the active grid also causes a modulation of the mean flow. This is due to the variable open area as function of the rotation angle of the disk. In figure 4 a graph of the open area of the grid in mm^2 is shown. On top of the mean value a slight modulations with an amplitude of approximately 0.4% is present. The lower graph of figure 4, which shows the amplitude of the Fourier transform of the open area signal, reveals the frequencies induces by the active grid. On the frequency axis a normalized frequency is used which is the frequency divided by the rotation frequency of the disk. The induced frequencies appear in multiples of five,

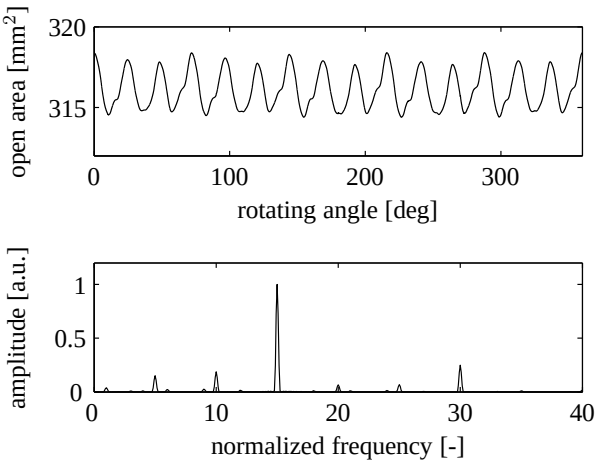

Figure 4: Open area signal when the disks from figure 3 are placed on top of each other. Top: Area open for flow to pass through as function of the rotation angle of the disk. Bottom: Fourier transform of open area signal.

since five spiral shaped slots are used.

In the work of Cekli et al. [8] a much larger mean open area modulation amplitude is used, in the order of 20%, but in the present study the goal is to only apply large scale time dependent forcing in the form of pulsating jets, while the mean flow rate is kept relatively constant. Large flow pulsations will give rise to acoustic coupling and combustion instabilities, which should be avoided. Besides the here presented geometry of the active grid, also geometries without spiral shaped slots will be used in future research. Here sets of two perforated disks are used and by varying the number and sizes of the perforations different open area signals are constructed, with either high or low modulation amplitude and with different frequencies.

The turbulence that is generated with the active grid is studied with hot-wire constant temperature anemometry (CTA). A single Dantec 90C10 CTA module is used in combination with local manufactured straight probes. The hot-wire probe is created from 5μm diameter platinum coated tungsten wire with a length of approximately 1mm.

The overheat ratio $a = (R_{hot} - R_{cold})/R_{cold}$ is set to 0.8, which means that the sensor has a temperature of approximately 220 degrees centigrade. To determine the frequency response of the hot-wire, the internal square wave test is used and this indicates a bandwidth of 75kHz.

In order to maximize the resolution of the measurements, the CTA output signal is rescaled by applying an offset and a gain to fully use the -10V to +10V range of the National Instruments 9215A BNC data acquisition device. The data is captured at 50kHz with 16bit dynamic range and afterwards low-pass filtered at 10kHz.

To convert the voltage to velocity a fourth order polynomial is fit through the calibration points. Velocities between 0.1 and 1 m/s are obtained by applying a calibrated volume flow through a straight pipe such that a laminar velocity profile develops of which the central velocity is known. The high velocity range, between 3 and 40m/s is obtained using a calibration nozzle with a cross section of 60mm^2. The velocity at the exit of the nozzle is obtained by registering the pressure difference over the nozzle with a betz manometer, which has a resolution better that 1Pa. Applying this pressure to Bernoulli's principle results in a velocity of $U = \sqrt{2p/\rho}$. The fourth order polynomial has an averaged error of less than 1% and a coefficient of determination, R^2, of 0.999.

Results

The first experiments with the designed active grid aim on achieving resonant turbulence. To that end the swirler geometry is excluded from the setup and the effect of the active grid is isolated. A constant flow of air is supplied to the setup by setting a pressure of three bar upstream of the calibrated orifice. This results in a center line velocity of approximately 8m/s. A frequency scan is made from 0 to 30Hz in steps of 2Hz and the hot-wire velocity signal is retrieved at 10mm above the outlet plane at the central axis. During combustion this is the location where the flame will stabilize. All measurements consist of 320 seconds of data to ensure properly converged statistics.

The phase averaged velocity of the different measurements reveals the different responses of the flow to the presence of the active grid. The phase averaged velocities are obtained with the use of the optical encoder to keep track of the absolute angular position of the rotating disk. Even a small error in the rotation speed will lead to significant errors over the long integration time. In figure 5 the phase averaged velocity of a few measurements are shown. Each measurement is shifted vertically with an offset to enhance the readability. At low frequency the flow tends to follow the normalized frequency of 15 that is applied by the time dependent open area of the grid, while at higher rotation frequencies this effect is damped and a oscillation with a five periods per rotation is experienced. The fact that the modulation of the grid open area cannot be followed at higher frequencies is completely in accordance with the wind tunnel experiments of Cekli et al. [8]. The normalized frequency of five at higher frequency is consistent with the jet frequency, which although created at the grid, is still present at the location of the flame. The graphs of figure 5 are each phase-shifted by $\phi_{shift} = 360hf/\bar{U}$ to compensate for the time delay due to the advection of the perturbation from the grid to the position of the wire.

In the graphs of figure 6 the energy spectra from the velocity signals are depicted, which are obtained from the power spectral density function of the velocity signals by the following equation.

$$E = |\mathcal{F}(u)|^2 \tag{1}$$

From these graphs it can be seen how the energy is distributed over the different time scales. The different rotations speeds are plotted with an offset factor for clearness

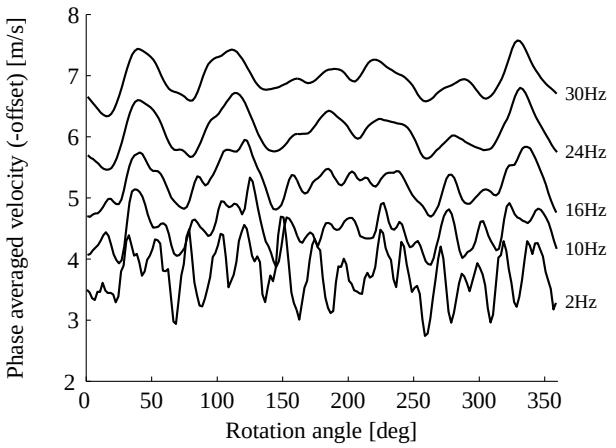

Figure 5: Phase averaged velocity at different rotation frequencies. The different measurements are shifted vertically by an offset. 30Hz: 0m/s, 24Hz: -1m/s, 16Hz: -2m/s, 10Hz: -3m/s, 2Hz: -4m/s

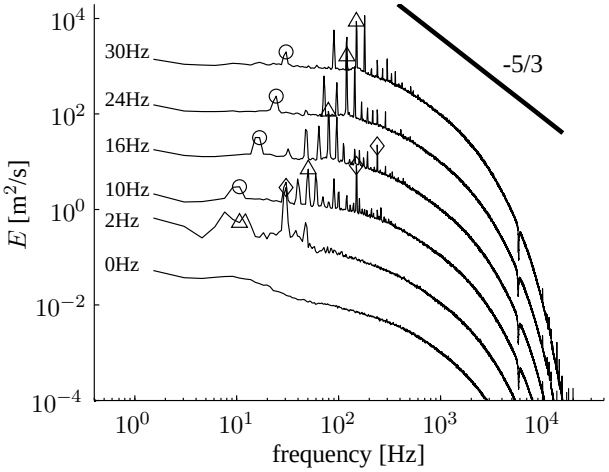

Figure 6: Energy spectra of velocity signal at different rotation frequencies. Peaks originating from the different normalized frequencies are labeled: 1 - circle, 5 - triangle, 15 - diamond. Spectra are shifted vertically with a factor. 2Hz: $\times 10$, 10Hz: $\times 10^2$, 16Hz: $\times 10^3$, 24Hz: $\times 10^4$ and 30Hz: $\times 10^5$

of the graph. The straight line indicates the -5/3 inertial range.

The results for the different measurements show that the inertial range is merely influenced by the different excitation frequencies, which indicates that no distinct scale in the inertial range is introduced. The only effect is a higher level of the spectrum for a wide range. On the large scales on the other hand there is clearly energy added in distinct scales. For low rotation frequencies the normalized frequency of 15 is present in the measurement signal, indicated with diamonds, and diminishes at higher excitation frequencies. Here the jet frequency at a normalized frequency of five, indicated with a triangle, is visible. Besides the frequencies of which the origin can be traced to the normalized frequencies induced by the grid, which are either the modulating open area or the pulsating jets, also other peaks are present. The rotation frequency itself can be observed; these peaks are indicated with a circle in figure 6. Integer multiples of the rotation frequency show up in the spectra. Especially three, four and six times the rotation frequency have a strong presence. Most likely this is due to eccentricity of the rotating plate, since a small misalignment introduces additional peaks to the graph of figure 4.

From the spectra it becomes clear that the active grid is capable of introducing specific scales to the flow at a downstream position. By integrating the difference between the spectra of the rotating grid measurements and the non-rotating measurement the amount of turbulent kinetic energy added is obtained. For a rotation of 2Hz speed this is 20% of the total turbulent kinetic energy and this decreases to 2.5% at 30Hz.

Since from previous studies it became clear that the optimal frequency to excite the flow is closely related to the large eddy turn over time, this quantity is calculated for the here described flow. The large eddy turn over time is defined by eq.2, which is the ratio of the integral length scale and the r.m.s. of the velocity fluctuations. To determine the integral length scale the integral of the autocorrelation is calculated (eq.3), which gives a measure for the largest structures present in the flow. The autocorrelation is calculated by the inverse Fourier transform of the power spectral density function (eq.4). To obtain the velocity as a function of the position use is made of Taylor's frozen turbulence approximation, $x = \overline{U}t$, which is a reasonable approximation at the experienced turbulence levels of 9%.

$$\tau = l_0/u' \tag{2}$$

$$l_0 = \int_0^\infty R(r)dr \tag{3}$$

$$R(r) = \overline{u(x)u(x+r)} = \mathcal{F}^{-1}\left\{\mathcal{F}\left(u\right)\mathcal{F}^*\left(u\right)\right\} \tag{4}$$

The integral length scale and the r.m.s. of the velocity fluctuations varies little with excitation frequency. The integral length scale varies from 15mm at 2Hz to 10mm at 30Hz and the r.m.s. of the velocity fluctuations vary from 0.86m/s to 0.75m/s. In the insert of figure 7 the eddy turn over time is shown, which varies between 12 and 18ms. In terms of a frequency to stir the turbulence, a response maximum is expected when the flow is excited between 55 and 83Hz.

To determine whether there is a resonance occurring, the mean eddy dissipation rate ε, defined by eq.5, is calculated for the different rotation frequencies.

$$\varepsilon = 15\nu\overline{\left(\frac{\partial u}{\partial x}\right)^2} \tag{5}$$

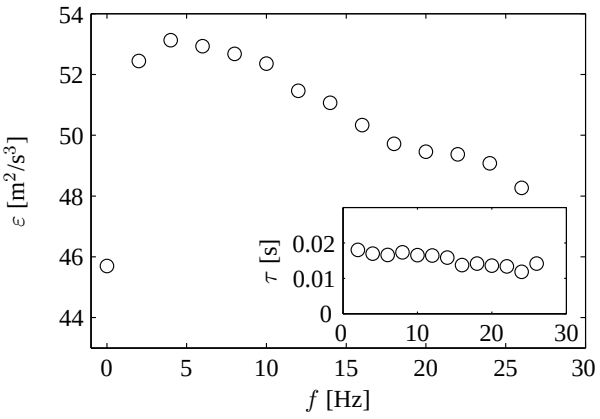

Figure 7: Mean eddy dissipation rate. Insert: Large eddy turn over time.

It is ε that determines the turbulence on scales in the inertial range up to the dissipation of the smaller eddies. This is most clear from the energy-spectrum function $E(\kappa) = C\varepsilon^{2/3}\kappa^{-5/3}$ that describes the energy distribution in inertial range by only ε and the universal Kolmogorov constant C as function of the wave number κ [10].

As can be seen in figure 7, the eddy dissipation rate increases when the active grid is set to operate. Although the resolution in rotation frequency is limited there is a response maximum visible near 4Hz, where ε is 15% higher than the stationary situation. The time scale of 60Hz that is introduced by the modulating open area of the grid, with normalized frequency of 15, corresponds very well with the inverse of the eddy turn over time. At higher rotation frequencies this modulation is damped by the flow, but the effect with lower normalized frequencies is more pronounced. Although also this effect introduces frequencies in the flow field close to the large eddy turn over time, there is no enhancement of the eddy dissipation rate.

Conclusions

The active grid with periodically open and closing holes by means of a perforated plate and a spiral shaped disk rotating in front is capable of introducing large scale perturbations to the flow. At low rotation speed the strongest frequencies present in the flow are induced by the modulation of the open flow area. This is most clear from the phase averaged velocity that follows a 15 periods oscillation per rotation. At higher rotation frequencies the effect of the modulated open flow area is damped and the pulsation frequency, with a normalized frequency of five is present in the flow. The other peaks that are visible in the spectra, all integer multiples of the rotation frequency, are most likely caused by the eccentricity of the two disks.

A maximum in the eddy dissipation rate is observed at approximately 4Hz and the strongest frequency that is induced is close to the large eddy turn over time as expected by several numerical and experimental studies. Since the maximum in the eddy dissipation rate is not very strong and since the resolution in frequency is limited, more experiments are needed to confirm the presence of a response maximum caused by the active grid. At higher rotation frequencies also a response maximum is expected, caused by the pulsating jets, but for this case no enhancement is observed.

Additional experiments are needed to test if the introduced scales will persist once the swirler geometry is inserted after the active grid. Since a substantial part of the turbulent kinetic energy is allocated in the large scales, experiments involving OH- and CH-PLIF will be used to determine the effect of these introduced scales on the formation of flame surface.

Acknowledgement

This project is sponsored by Technology Foundation STW, The Netherlands.

Nomenclature

a	Over heat ratio	-
E	Energy spectrum	m^2/s
f	Rotation frequency of grid	Hz
$\mathcal{F}$	Fourier transform	-
h	Distance between active grid and hot-wire	m
l_0	Integral length scale	m
$R(r)$	Auto-correlation function	m^2/s^2
$R_{cold/hot}$	Resistance of hot-wire at room temperature / operating temperature	Ω
t	Time	s
u	Instantaneous velocity fluctuation	m/s
u'	R.m.s. of velocity fluctuations	m/s
$\bar{U}$	Mean velocity	m/s
U	Instantaneous velocity	m/s
x	Position	m
ε	Mean eddy dissipation rate	m^2/s^3
ν	Kinematic viscosity	m^2/s
τ	Large eddy turn over time	s
ϕ_{shift}	Phase shift	deg

References

[1] K. Döbbeling, J. Hellat, H. Koch, 25 years of bbc/abb/alstom lean premix combustion technologies, Journal of Engineering for Gas Turbines and Power 129 (1) (2007) 2–12. doi:10.1115/1.2181183.

[2] R. Cheng, D. Yegian, M. Miyasato, G. Samuelsen, C. Benson, R. Pellizzari, P. Loftus, Scaling and development of low-swirl burners for low-emission furnaces and boilers, Proceedings of the Combustion Institute 28 (1) (2000) 1305–1313. doi:10.1016/S0082-0784(00)80344-6.

[3] D. Littlejohn, R. Cheng, Fuel effects on a low-swirl

injector for lean premixed gas turbines, Proceedings of the Combustion Institute 31 (2) (2007) 3155–3162. doi:10.1016/j.proci.2006.07.146.

[4] R. Cheng, H. Levinsky, Lean Combustion: Technology and Control, Elsevier, Inc, 2008, Ch. 6 - Lean Premixed Burners.

[5] A. K. Kuczaj, B. J. Geurts, D. Lohse, Response maxima in time-modulated turbulence: Direct numerical simulations, Europhysics Letters 73 (6) (2006) 851–857. doi:10.1209/epl/i2005-10486-2.

[6] D. Lohse, Periodically kicked turbulence, Physical Review E 64 (4) (2000) 4946–4949. doi:10.1103/PhysRevE.62.4946.

[7] O. Cadot, J. H. Titon, D. Bonn, Experimental observation of resonances in modulated turbulence, Journal of Fluid Mechanics 485 (2003) 161–170. doi:10.1017/S0022112003004592.

[8] H. E. Cekli, C. Tipton, W. van de Water, Resonant enhancement of turbulent energy dissipation, Physical Review Letters 105 (2010) 044503. doi:10.1103/PhysRevLett.105.044503.

[9] H. Makita, Realization of a large scale turbulence field in a small wind tunnel, Fluid Dynamics Research 8 (1-4) (1991) 53–64. doi:10.1016/0169-5983(91)90030-M.

[10] S. B. Pope, Turbulent Flows, Cambridge University Press, 2006.